Joint Symbol-Level Precoding and Reflecting Designs for IRS-Enhanced MU-MISO Systems

Rang Liu, *Graduate Student Member, IEEE*, Ming Li, *Senior Member, IEEE*, Qian Liu, *Member, IEEE*, and A. Lee Swindlehurst, *Fellow, IEEE*

***Abstract*— Intelligent reflecting surfaces (IRSs) have emerged as a revolutionary solution to enhance wireless communications by changing propagation environment in a cost-effective and hardware-efficient fashion. In addition, symbol-level precoding (SLP) has attracted considerable attention recently due to its advantages in converting multiuser interference (MUI) into useful signal energy. Therefore, it is of interest to investigate the employment of IRS in symbol-level precoding systems to exploit MUI in a more effective way by manipulating the multiuser channels. In this article, we focus on joint symbol-level precoding and reflecting designs in IRS-enhanced multiuser multiple-input single-output (MU-MISO) systems. Both power minimization and quality-of-service (QoS) balancing problems are considered. In order to solve the joint optimization problems, we develop an efficient iterative algorithm to decompose them into separate symbol-level precoding and block-level reflecting design problems. An efficient gradient-projection-based algorithm is utilized to design the symbol-level precoding and a Riemannian conjugate gradient (RCG)-based algorithm is employed to solve the reflecting design problem. Simulation results demonstrate the significant performance improvement introduced by the IRS and illustrate the effectiveness of our proposed algorithms.**

***Index Terms*— Intelligent reflecting surface (IRS), symbol-level precoding (SLP), multiuser multiple-input single-output (MU-MISO) systems, manifold optimization.**

Manuscript received March 18, 2020; revised July 18, 2020; accepted September 28, 2020. Date of publication October 9, 2020; date of current version February 11, 2021. This work was supported in part by the National Natural Science Foundation of China under Grant 61671101, Grant 61971088, Grant 62071083, and Grant 61761136019; in part by the Fundamental Research Funds for the Central Universities under Grant DUT20GJ214 and Grant DUT18RC(3)069; and in part by the Dalian Science and Technology Innovation Project under Grant 2020JJ25CY001. The work of A. Lee Swindlehurst was supported by the National Science Foundation under Grant CCF-2008724 and Grant ECCS-2030039. This article was presented in part at the IEEE Wireless Communications and Networking Conference (WCNC), 2020. The associate editor coordinating the review of this article and approving it for publication was G. C. Alexandropoulos. *(Corresponding author: Ming Li.)*

Rang Liu and Ming Li are with the School of Information and Communication Engineering, Dalian University of Technology, Dalian 116024, China (e-mail: liurang@mail.dlut.edu.cn; mli@dlut.edu.cn).

Qian Liu is with the School of Computer Science and Technology, Dalian University of Technology, Dalian 116024, China (e-mail: qianliu@dlut.edu.cn).

A. Lee Swindlehurst is with the Center for Pervasive Communications and Computing, University of California at Irvine, Irvine, CA 92697 USA (e-mail: swindle@uci.edu).

Color versions of one or more of the figures in this article are available online at https://ieeexplore.ieee.org.

Digital Object Identifier 10.1109/TWC.2020.3028371

I. Introduction

During the past decade, the applications of wireless communications have been growing rapidly and now affect nearly every aspect of our daily life. Meanwhile, the demands of wireless communication networks for high data rate and low latency are also continuously increasing. Various technical solutions have been proposed to meet the requirements of fifth-generation (5G) networks and beyond. Among those technologies, massive multi-input multi-output (MIMO), millimeter wave (mmWave) communications, and ultra-dense networks are deemed as three fundamental approaches to enhance the performance along three basic dimensions: Improving spectral efficiency, utilizing more spectrum, and exploiting spatial reuse [2], [3]. However, it seems that the performance improvements offered by these approaches are reaching their limits, and new technologies in different directions are needed to achieve further fundamental advances in wireless networks. One such technology is the use of intelligent reflecting surfaces (IRS), which is a potentially revolutionary approach that provides additional degrees of freedom in system design by intelligently changing the propagation environment [4]–[8].

An IRS is a planar array composed of a large number of reconfigurable passive reflecting elements, which are made up of some hardware-efficient devices, e.g., positive-intrinsic-negative (PIN) diodes and phase shifters. Each reflecting element can independently and intelligently manipulate the amplitude and/or phase of incident electromagnetic (EM) waves in a programmable manner, which can produce a favorable propagation environment, especially when faced with blockages or severe fading. New research on micro-electrical-mechanical systems (MEMS) and meta-materials has enabled the IRS to be configured in real-time, which is necessary for the rapidly changing wireless communication environment. Thus, IRS have the potential for greatly expanding coverage, improving transmission quality, and enhancing security, etc., in a cost-effective and hardware-efficient fashion. Moreover, these lightweight devices can be easily attached to the surfaces of buildings or mobile equipment, which provides mobility and portability for practical implementation [5], [6].

Attracted by above advantages, researchers have devoted considerable attention to the development of IRS in the

past year. The applications of IRS to different wireless systems have been investigated to enhance their performance with different performance goals [9]–[30]. By properly designing the phase-shifting components of the IRS, the reflected signals can be coherently added to the received signals from other paths at intended receivers, which facilitates minimization of the transmit power [9], [10], or improving transmission performance in terms of spectral efficiency [11], [12], energy reception [13], ergodic capacity [14], symbol error rate [15], channel capacity [16], sum-rate [17]–[19], and power efficiency [20], etc. IRS-enhanced physical layer security has been investigated in [21]–[23]. In order to provide preferable performance, the required number of reflecting elements has been studied in [24], [25]. For practical implementation, researchers have investigated the applications of IRS with limited-resolution phase shifters [26]–[29] and phase errors [30]. The IRS technique was also employed to realize index modulation [31], passive information transmission [32], [33], and holographic massive MIMO [34]. Advanced machine learning-based algorithms have also been utilized to solve optimization problems related to IRS-assisted systems [35], [36]. In addition, practical channel estimation algorithms for IRS-assisted wireless communication systems have been proposed in [37]–[40].

Precoding design is also of significant importance to facilitate information transmissions in IRS-enhanced multi-user systems. In existing works, multi-user interference (MUI) is regarded as a harmful component and suppressed by the precoding and reflecting designs as much as possible. However, recent research [41]–[45] has found that MUI can often be treated as a source of useful signal energy to enhance information transmissions by means of symbol-level precoding techniques. Specifically, symbol-level precoding utilizes transmitted symbol information and channel state information (CSI) to design the precoder, which converts harmful MUI into constructive interference to improve the symbol detection performance compared with linear block-level precoding.

Motivated by these findings, we propose to combine symbol-level precoding and IRS in order to enjoy the advantages of both technologies. The employment of IRS can facilitate the exploitation of MUI in symbol-level precoding by favorably manipulating the multi-user propagation channels. However, there are some obstacles that must be tackled. First, the symbol-level precoder changes with each transmitted symbol vector, while the IRS reflects all of them with the same phase-shift beamforming. Thus, symbol-level constraints are difficult to implement in the reflecting design. Since both the symbol-level precoding and reflecting need to consider all possible transmit vectors, the computational complexity will be tremendously high for large-scale systems and high-level modulation types. To the best of our knowledge, this problem has not been studied yet, which motivates the work in this article.

We consider the joint design of symbol-level precoding and IRS transmission design in multi-user multi-input single-output (MU-MISO) systems. In particular, we consider a multi-antenna base station (BS) serving a number of single-antenna users with the aid of an IRS, which consists of many reflecting elements. Our goal is to design the symbol-level precoder and IRS reflection to enhance the system performance by exploiting both MUI and modifications to the propagation environment. The main contributions in this article are summarized as follows:

- We first focus on power minimization problem, which attempts to minimize the average transmit power as well as guarantee a certain quality-of-service (QoS) for the information transmissions. In order to solve this joint design problem, an efficient iterative algorithm is proposed to decompose the problem into separate symbol-level precoding and reflecting designs, where the gradient-projection-based and Riemannian conjugate gradient (RCG)-based algorithms are exploited.
- Then, we investigate the QoS balancing problem, which aims at maximizing the minimum QoS among users with a given average power constraint. The symbol-level precoding and reflecting are iteratively updated using similar gradient-projection-based and RCG-based algorithms after some transformations.
- Finally, we provide extensive simulation results to evaluate the performance of the proposed IRS-enhanced systems and the effectiveness of proposed algorithms. In particular, we show that applying IRS to symbol-level precoding MU-MISO systems brings remarkable performance improvements in terms of power-savings and symbol error rate (SER)-reduction, which illustrates how IRS have a positive effect on interference exploitation as well as the symbiotic benefits of using IRS and symbol-level precoding together.

The rest of this article is organized as follows. Section II introduces the system model of our proposed IRS-enhanced MU-MISO system. The considered power minimization and QoS balancing problems are investigated in Sections III and IV, respectively. The algorithm initialization and complexity analysis are presented in Section V. Simulation results are presented in Section VI, and finally conclusions are provided in Section VII.

The following notation is used throughout this article. Boldface lower-case and upper-case letters indicate column vectors and matrices, respectively. $(\cdot)^T$ and $(\cdot)^H$ denote the transpose and the transpose-conjugate operations, respectively. $\mathbb{C}$ denotes the set of complex numbers. $|a|$ and $\|\mathbf{a}\|$ are the magnitude of a scalar a and the norm of a vector $\mathbf{a}$, respectively. $\angle a$ is the angle of complex-valued a. $\Re\{\cdot\}$ and $\Im\{\cdot\}$ denote the real and imaginary part of a complex number, respectively. $\mathrm{diag}\{\mathbf{a}\}$ indicates the diagonal matrix whose diagonals are the elements of $\mathbf{a}$. $\mathbf{A} \succeq \mathbf{0}$ indicates that the matrix $\mathbf{A}$ is positive semi-definite. Finally, we adopt the following indexing notation: $\mathbf{A}(i,j)$ denotes the element of the i-th row and the j-th column of matrix $\mathbf{A}$, and $\mathbf{a}(i)$ denotes the i-th element of vector $\mathbf{a}$.

II. System Model

We consider an IRS-enhanced MU-MISO system as shown in Fig. 1, where a BS equipped with M antennas serves K single-antenna users with the aid of an IRS. The IRS consists of N passive reflecting elements, which are implemented by

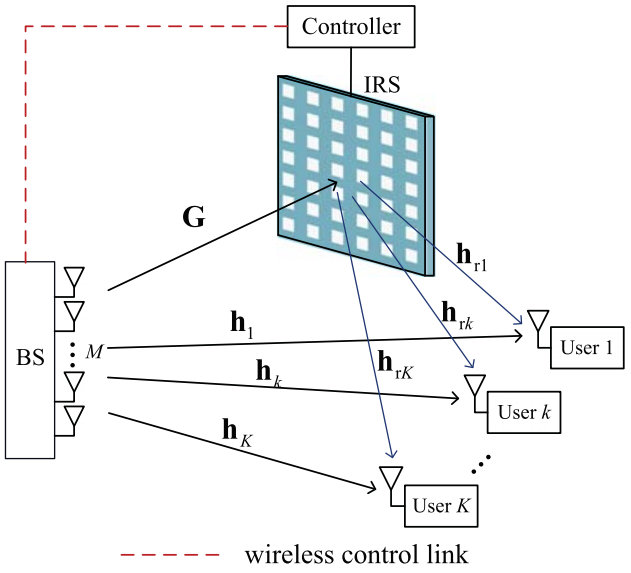

Fig. 1. The IRS-enhanced MU-MISO system.

phase shifters and denoted as $\boldsymbol{\theta} \triangleq [\theta_1, \ldots, \theta_N]$ that satisfy[1] $|\theta_n| = 1, \forall n$. Each reflecting element is adaptively adjusted by the controller, which receives information about the optimized phase shifts from the BS through a dedicated control link. We denote $\mathbf{G} \in \mathbb{C}^{N \times M}$, $\mathbf{h}_k \in \mathbb{C}^{M \times 1}$, and $\mathbf{h}_{rk} \in \mathbb{C}^{N \times 1}$ as the channels from BS to IRS, from BS to the k-th user and from IRS to the k-th user, respectively. In this article, we assume that the CSI of all channels is known perfectly and instantaneously to the BS.[2]

To facilitate the symbol-level precoding technique, we assume the transmitted symbols are independently selected from a Ω-phase shift keying (PSK) constellation[3] (i.e., $\Omega = 2, 4, \ldots$). Therefore, the transmitted symbol vector $\mathbf{s}_m \triangleq [s_{m,1}, \ldots, s_{m,K}]$ has Ω^K combinations, i.e., $m = 1, \ldots, \Omega^K$. For different $\mathbf{s}_m$, the BS changes its transmitted precoder vector $\mathbf{x}_m \in \mathbb{C}^{M \times 1}$ in order to exploit the MUI. Unlike conventional linear block-level precoding techniques, the mapping from $\mathbf{s}_m$ to $\mathbf{x}_m$ is usually nonlinear.

Through the direct and reflected paths, the compound received signal at the k-th user can be written as

$$r_{m,k} = \left(\mathbf{h}_k^H + \mathbf{h}_{rk}^H \boldsymbol{\Theta} \mathbf{G}\right) \mathbf{x}_m + n_k, \forall m, \tag{1}$$

[1]In this preliminary work, we adopt the popular ideal phase-shift model [9]–[25] which indicates a constant amplitude for all phase shifts. In actual implementations, the reflection amplitudes will vary with the value of the phase shifts [27], and these variations are associated with the difference between the frequency of the incident wave and the resonant frequency of the reflecting circuit [28]. Research assuming more realistic models will be conducted in future investigations.

[2]In practice, channel estimation for IRS-enhanced systems is challenging since the passive reflecting elements in general do not have the ability to sense and process the received signals. Although some initial channel estimation approaches [37]–[40] have been proposed, CSI is still difficult to obtain with limited overhead. In order to focus on the impact of joint symbol-level precoding and reflecting problems, we assume perfect CSI in this article. Problems involving imperfect CSI or no CSI are left for future studies.

[3]We should emphasize that symbol-level precoding is related to the modulation type. Therefore, our designs in this article are only capable of exploiting PSK modulation. The design for QAM modulation will be investigated in future work.

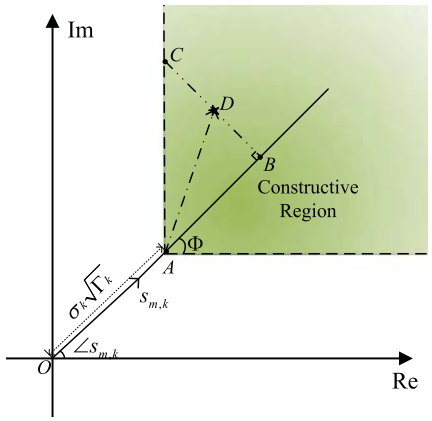

(a) An example of the constructive region.

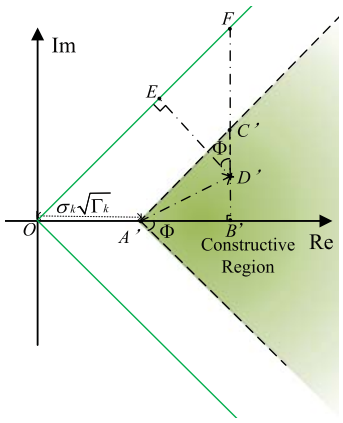

(b) After rotating the diagram in Fig. 2(a) clockwise by $\angle s_{m,k}$ degrees.

Fig. 2. Constructive region for a QPSK symbol.

where $\boldsymbol{\Theta} \triangleq \mathrm{diag}\{\boldsymbol{\theta}\}$ denotes the phase shifts of the IRS, and $n_k \sim \mathcal{CN}(0, \sigma_k^2)$ is additive white Gaussian noise (AWGN) for the k-th user. Moreover, it is noteworthy that, during a coherent time slot with the same CSI, the BS changes $\mathbf{x}_m$ according to the transmitted symbols while the IRS phase shifts $\boldsymbol{\theta}$ remain unchanged. Therefore, the reflecting design should consider all possible Ω^K precoding vectors. Defining the precoding matrix $\mathbf{X} \triangleq [\mathbf{x}_1, \ldots, \mathbf{x}_{\Omega^K}]$, the average transmit power required to send a given symbol vector is

$$P_{\mathrm{ave}} = \frac{\|\mathbf{X}\|_F^2}{\Omega^K}. \tag{2}$$

With knowledge of the symbols to be transmitted, symbol-level precoding makes the MUI constructive to the information transmissions by elaborately designing $\mathbf{x}_m$. In particular, the MUI is converted into constructive interference if it can push the received signals away from the PSK decision boundaries. In order to illustrate the idea behind constructive interference, without loss of generality, we take quadrature phase shift keying (QPSK) as an example ($\Omega = 4$). For simplicity, we also consider $\left(\frac{1}{\sqrt{2}}, \frac{1}{\sqrt{2}}j\right)$ as the symbol of interest for the k-th user and show the received signal in the complex plane as in Fig. 2(a). Since the decision boundaries for this symbol of interest are the positive halves of the x and y

axes, as long as the noise-corrupted received signal expressed in (1) is in the first quadrant, the receiver can correctly detect the desired signal. However, when we design the precoder $\mathbf{x}_m$, the noise is unknown and cannot be predicted beforehand.

Denote the received noise-free signal of the k-th user as

$$\widetilde{r}_{m,k} = \left(\mathbf{h}_k^H + \mathbf{h}_{\mathrm{r}k}^H \boldsymbol{\Theta}\mathbf{G}\right)\mathbf{x}_m, \tag{3}$$

which is illustrated as point D in Fig. 2(a). To reduce the impact of noise on the symbol detection, it is desirable to design $\mathbf{x}_m$ such that point D is sufficiently far away from the corresponding decision boundaries to satisfy the QoS. In order to quantify the QoS requirement, let Γ_k be the signal-to-noise ratio (SNR) requirement for the k-th user. If we ignore the impact of MUI and focus on the single-user case, the received noise-free signal should be at point A to ensure that $\frac{|\widetilde{r}_{m,k}|^2}{\sigma_k^2} = \Gamma_k$, i.e., $\overrightarrow{OA} = \sigma_k\sqrt{\Gamma_k}\mathbf{s}_m(k)$. Considering the multi-user signal as in (1), symbol-level precoding aims to design $\mathbf{x}_m$ such that point D lies in the constructive (green) region, where the distance between received signal and its decision boundaries, which can be expressed as $\sigma_k\sqrt{\Gamma_k}\cos\Phi$, is guaranteed to satisfy the SNR requirement. Therefore, symbol-level precoding can achieve better SER performance by converting the MUI into a constructive component.

In order to geometrically express this relationship, we project point D on the direction of $\overrightarrow{OA}$ at point B, and define point C to be the intersection of the extension of $\overrightarrow{BD}$ and the boundaries of the constructive region. Then, the received noise-free signal in the green region should satisfy

$$\left|\overrightarrow{BC}\right| - \left|\overrightarrow{BD}\right| \geq 0. \tag{4}$$

To make this expression clearer, we rotate the diagram in Fig. 2(a) clockwise by $\angle s_{m,k}$ degrees as shown in Fig. 2(b). Then, the QoS requirement is readily expressed as

$$\left[\Re\left\{\widetilde{r}_{m,k}e^{-j\angle s_{m,k}}\right\} - \sigma_k\sqrt{\Gamma_k}\right]\tan\Phi \\ \left|\Im\left\{\widetilde{r}_{m,k}e^{-j\angle s_{m,k}}\right\}\right| \geq 0, \forall k, \forall m. \tag{5}$$

In this article, we consider two typical optimization problems for IRS-enhanced MU-MISO systems: *i*) the power minimization problem, which minimizes the average transmit power while guaranteeing the QoS of the data received by the users; *ii*) the QoS balancing problem, which aims to maximize the minimum QoS with a given average transmit power budget. In the following sections, we will formulate and solve these two problems.

III. Algorithm for Power Minimization Problem

With the previous analysis, the average power minimization problem can be written as

$$\min_{\mathbf{X},\boldsymbol{\theta}} \quad \|\mathbf{X}\|_F^2 \tag{6a}$$

$$\text{s.t.} \left[\Re\left\{\widetilde{r}_{m,k}e^{-j\angle s_{m,k}}\right\} - \sigma_k\sqrt{\Gamma_k}\right]\tan\Phi \\ - \left|\Im\left\{\widetilde{r}_{m,k}e^{-j\angle s_{m,k}}\right\}\right| \geq 0, \quad \forall k,\ \forall m, \tag{6b}$$

$$\widetilde{r}_{m,k} = \left(\mathbf{h}_k^H + \mathbf{h}_{\mathrm{r}k}^H\boldsymbol{\Theta}\mathbf{G}\right)\mathbf{x}_m, \quad \forall k,\ \forall m, \tag{6c}$$

$$\boldsymbol{\Theta} = \mathrm{diag}\{\boldsymbol{\theta}\}, |\theta_n| = 1, \quad \forall n, \tag{6d}$$

which is non-convex due to the IRS constraints (6d). Furthermore, the size of $\mathbf{X} \in \mathbb{C}^{M\times\Omega^K}$ is very large even for relatively small K and Ω. Thus, it is difficult to directly solve this large-scale joint symbol-level precoding and reflecting problem. In order to tackle this difficulty, we propose to decompose this bivariate problem into two sub-problems and implement the solutions iteratively.

A. Symbol-Level Precoding Design for Power Minimization Problem

When the IRS phase shifts $\boldsymbol{\theta}$ are fixed, the overall channel vector is determined. We denote the combined channel vector from the BS to the k-th user as $\widetilde{\mathbf{h}}_k^H \triangleq \mathbf{h}_k^H + \mathbf{h}_{\mathrm{r}k}^H\boldsymbol{\Theta}\mathbf{G}, \forall k$. Since the precoder vectors $\mathbf{x}_m, m = 1,\ldots,\Omega^K$, are independent of each other, the power minimization problem (6) can be divided into Ω^K sub-problems. The m-th sub-problem for optimizing $\mathbf{x}_m$ is given by

$$\min_{\mathbf{x}_m} \quad \|\mathbf{x}_m\|^2 \tag{7a}$$

$$\text{s.t.} \left[\Re\left\{\widetilde{\mathbf{h}}_k^H\mathbf{x}_m e^{-j\angle s_{m,k}}\right\} - \sigma_k\sqrt{\Gamma_k}\right]\tan\Phi \\ - \left|\Im\left\{\widetilde{\mathbf{h}}_k^H\mathbf{x}_m e^{-j\angle s_{m,k}}\right\}\right| \geq 0, \quad \forall k. \tag{7b}$$

This is a convex optimization problem and can be solved by standard convex tools, e.g., the CVX solver [46]. In addition, an efficient gradient projection algorithm with low complexity has also been studied in [41], which converts the problem to real-valued notation, and then derives its Lagrangian dual function to facilitate the gradient projection algorithm. Due to space limitations, details of the algorithm to solve (7) are omitted.

B. Reflecting Design for Power Minimization Problem

After obtaining the precoder vectors $\mathbf{x}_m, m = 1,\ldots,\Omega^K$, the objective of the original optimization problem (6) has been determined. This means that, with given $\mathbf{x}_m$, the design of the reflection coefficients $\boldsymbol{\theta}$ becomes a feasibility-check problem whose outcome will not directly affect the power minimization objective of (6). Therefore, for the reflecting design, we formulate another proper objective function that enhances the reduction of the transmit power for future iterations and guarantees its feasibility.

Since the power minimization problem (7) is convex, the optimal $\mathbf{x}_m$ usually makes the left-hand side of constraint (7b) equal to a relatively small positive value, i.e., the QoS requirement is satisfied almost with equality. In order to further reduce the transmit power in the next iteration, we propose to design the IRS phase shifts $\boldsymbol{\theta}$ using the stricter constraint (8b) in place of (7b), which can introduce an improved QoS that can provide more freedom for power minimization in the next iteration. To this end, the IRS reflecting design problem is transformed to

$$\max_{\boldsymbol{\theta},\alpha_{m,k}} \quad \sum_{m=1}^{\Omega^K}\sum_{k=1}^{K}\alpha_{m,k} \tag{8a}$$

$$\text{s.t.} \left[\Re\left\{\widetilde{r}_{m,k}e^{-j\angle s_{m,k}}\right\} - \sigma_k\sqrt{\Gamma_k}\right]\tan\Phi \tag{8b}$$

$$-\left|\Im\left\{\widetilde{r}_{m,k}e^{-j\angle s_{m,k}}\right\}\right| \geq \alpha_{m,k}, \quad \forall k, \forall m,$$
$$\widetilde{r}_{m,k} = \left(\mathbf{h}_k^H + \mathbf{h}_{rk}^H \boldsymbol{\Theta}\mathbf{G}\right)\mathbf{x}_m, \quad \forall k, \forall m, \tag{8c}$$
$$\boldsymbol{\Theta} = \mathrm{diag}\{\boldsymbol{\theta}\}, |\theta_n| = 1, \quad \forall n, \tag{8d}$$

where the auxiliary variable $\alpha_{m,k}$ can be viewed as the residual QoS requirement. Then, by defining

$$a_{m,k} \triangleq \mathbf{h}_k^H \mathbf{x}_m e^{-j\angle s_{m,k}}, \quad \forall k, \forall m, \tag{9a}$$
$$\mathbf{b}_{m,k} \triangleq \mathrm{diag}\left\{\mathbf{h}_{rk}^H\right\}\mathbf{G}\mathbf{x}_m e^{-j\angle s_{m,k}}, \quad \forall k, \forall m, \tag{9b}$$
$$\widehat{r}_{m,k} \triangleq a_{m,k} + \boldsymbol{\theta}^H \mathbf{b}_{m,k}, \tag{9c}$$

problem (8) can be reformulated concisely as

$$\min_{\boldsymbol{\theta}} \sum_{m=1}^{\Omega^K}\sum_{k=1}^{K}\left|\Im\left\{\widehat{r}_{m,k}\right\}\right| - \left[\Re\left\{\widehat{r}_{m,k}\right\} - \sigma_k\sqrt{\Gamma_k}\right]\tan\Phi \tag{10a}$$
$$\text{s.t.} \quad |\theta_n| = 1, \quad \forall n. \tag{10b}$$

Unfortunately, the absolute values in the objective (10a) are non-differentiable, which hinders the algorithm development. In addition, the unit modulus constraints for the IRS phase shifts in (10b) introduce another difficulty due to their non-convexity. Thus, we turn to solving above two problems by the log-sum-exp and manifold-based algorithms in the followings.

In order to handle the absolute value terms, we approximate the objective (10a) by a differentiable function. It can be observed that (10a) can be concisely expressed as $|a|+b$, where a and b are scalars. Then, the non-differentiable absolute value function can be replaced by

$$|a| + b = \max\left\{a + b, -a + b\right\}. \tag{11}$$

We then exploit the well-known log-sum-exp method and obtain

$$\max\left\{a+b, -a+b\right\} \approx \varepsilon \log\left[\exp\left(\frac{a+b}{\varepsilon}\right) + \exp\left(\frac{-a+b}{\varepsilon}\right)\right], \tag{12}$$

where ε is a relatively small positive number to maintain the approximation. Thus, the optimization problem (10) can be reformulated as

$$\min_{\boldsymbol{\theta}} \quad g \triangleq \sum_{i=1}^{K\Omega^K} \varepsilon \log\left[\exp\left(\frac{f_{2i-1}}{\varepsilon}\right) + \exp\left(\frac{f_{2i}}{\varepsilon}\right)\right] \tag{13a}$$
$$\text{s.t.} \quad |\theta_n| = 1, \quad \forall n. \tag{13b}$$

For simplicity, in (13) we define $f_i, i = 1, 2, \ldots, K\Omega^K$, as

$$f_{2i-1} \triangleq \Im\left\{\widehat{r}_{m,k}\right\} - \left[\Re\left\{\widehat{r}_{m,k}\right\} - \sigma_k\sqrt{\Gamma_k}\right]\tan\Phi = \Re\{\boldsymbol{\theta}^H\}\mathbf{a}_{2i-1} + \Im\{\boldsymbol{\theta}^H\}\mathbf{b}_{2i-1} + c_{2i-1}, \tag{14a}$$
$$f_{2i} \triangleq -\Im\left\{\widehat{r}_{m,k}\right\} - \left[\Re\left\{\widehat{r}_{m,k}\right\} - \sigma_k\sqrt{\Gamma_k}\right]\tan\Phi = \Re\{\boldsymbol{\theta}^H\}\mathbf{a}_{2i} + \Im\{\boldsymbol{\theta}^H\}\mathbf{b}_{2i} + c_{2i}, \tag{14b}$$

where $i = K(m-1)+k$ and

$$\mathbf{a}_{2i-1} \triangleq \Im\{\mathbf{b}_{m,k}\} - \Re\{\mathbf{b}_{m,k}\}\tan\Phi, \tag{15a}$$
$$\mathbf{b}_{2i-1} \triangleq \Re\{\mathbf{b}_{m,k}\} + \Im\{\mathbf{b}_{m,k}\}\tan\Phi, \tag{15b}$$
$$c_{2i-1} \triangleq \Im\{a_{m,k}\} - \Re\{a_{m,k}\}\tan\Phi + \sigma_k\sqrt{\Gamma_k}\tan\Phi, \tag{15c}$$
$$\mathbf{a}_{2i} \triangleq -\Im\{\mathbf{b}_{m,k}\} - \Re\{\mathbf{b}_{m,k}\}\tan\Phi, \tag{15d}$$
$$\mathbf{b}_{2i} \triangleq -\Re\{\mathbf{b}_{m,k}\} + \Im\{\mathbf{b}_{m,k}\}\tan\Phi, \tag{15e}$$
$$c_{2i} \triangleq -\Im\{a_{m,k}\} - \Re\{a_{m,k}\}\tan\Phi + \sigma_k\sqrt{\Gamma_k}\tan\Phi. \tag{15f}$$

While the objective of (13) is smooth and differentiable, the unit modulus constraints (13b) are non-convex, which still makes the problem difficult to solve. Two popular methods for handling this type of constraint include non-convex relaxation and alternating minimization. However, the non-convex relaxation method always suffers a performance loss since the solution is based on a relaxation of the original problem. On the other hand, the alternating minimization method may have slow convergence due to the large number of variables involved. In order to deal with these difficulties, we adopt the Riemannian-manifold-based algorithm, which can achieve a locally optimal solution of the original optimization problem with very fast convergence [47].

Before developing the algorithm, we need to introduce some related concepts. On a manifold, each point has a neighborhood homeomorphic to Euclidean space, and the directions in which the point can move are its tangent vectors, which compose the tangent space. Similar to the Euclidean space, the tangent space has one tangent vector in the direction where the objective function decreases fastest, which is referred to as the Riemannian gradient. Furthermore, the Riemannian gradient is the orthogonal projection of the Euclidean gradient onto its corresponding tangent space. Therefore, efficient algorithms used in Euclidean space, e.g., the conjugate gradient (CG) and the trust-region methods, are suitable on the Riemannian manifold after several operations. In the following, we apply the conjugate gradient algorithm on the Riemannian manifold to solve our problem.

Denoting $\widetilde{\boldsymbol{\Theta}} \triangleq [\Re\{\boldsymbol{\theta}\}, \Im\{\boldsymbol{\theta}\}]^T$, the unit modulus constraints (13b) form a $2N$-dimensional smooth Riemannian manifold

$$\mathcal{M} = \left\{\widetilde{\boldsymbol{\Theta}} \in \mathbb{R}^{2\times N} : [\widetilde{\boldsymbol{\Theta}}(:,n)]^T\widetilde{\boldsymbol{\Theta}}(:,n) = 1, \forall n\right\}, \tag{16}$$

whose tangent space is

$$T_{\widetilde{\boldsymbol{\Theta}}}\mathcal{M} = \left\{\mathbf{P} \in \mathbb{C}^{2\times N} : [\widetilde{\boldsymbol{\Theta}}(:,n)]^T\mathbf{P}(:,n) = 0, \forall n\right\}. \tag{17}$$

In order to facilitate the conjugate gradient algorithm, the Euclidean gradient is required to determine the corresponding Riemannian gradient. Let $\widetilde{\boldsymbol{\theta}}_n$ be the n-th column of $\widetilde{\boldsymbol{\Theta}}$, so that the Euclidean gradient of $g(\widetilde{\boldsymbol{\Theta}})$ can be expressed as

$$\nabla_{\widetilde{\boldsymbol{\Theta}}} g = \left[\frac{\partial g}{\partial \widetilde{\boldsymbol{\theta}}_1}, \ldots, \frac{\partial g}{\partial \widetilde{\boldsymbol{\theta}}_N}\right]. \tag{18}$$

Following the chain rule, the n-th column of the Euclidean gradient is calculated as

$$\frac{\partial g}{\partial \widetilde{\boldsymbol{\theta}}_n} = \frac{\partial \Re\{\boldsymbol{\theta}^H\}}{\partial \widetilde{\boldsymbol{\theta}}_n}\left(\frac{\partial g}{\partial \Re\{\boldsymbol{\theta}^H\}}\right)^T + \frac{\partial \Im\{\boldsymbol{\theta}^H\}}{\partial \widetilde{\boldsymbol{\theta}}_n}\left(\frac{\partial g}{\partial \Im\{\boldsymbol{\theta}^H\}}\right)^T. \tag{19}$$

According to the previous definition, it is obvious that

$$\frac{\partial \Re\{\boldsymbol{\theta}^H\}}{\partial \widetilde{\boldsymbol{\theta}}_n} = [\mathbf{e}_n, \mathbf{0}]^T, \frac{\partial \Im\{\boldsymbol{\theta}^H\}}{\partial \widetilde{\boldsymbol{\theta}}_n} = [\mathbf{0}, \mathbf{e}_n]^T, \tag{20}$$

where $\mathbf{e}_n \in \mathbb{R}^{N\times 1}$ is defined by $\mathbf{e}_n(n) = 1, \mathbf{e}_n(i) = 0$, $\forall i \neq n$. Based on (13a) and (14), we have

$$\frac{\partial g}{\partial \Re\{\boldsymbol{\theta}^H\}} = \sum_{i=1}^{K\Omega^K} \frac{\exp(f_{2i-1}/\varepsilon)\mathbf{a}_{2i-1}^T + \exp(f_{2i}/\varepsilon)\mathbf{a}_{2i}^T}{\exp(f_{2i-1}/\varepsilon) + \exp(f_{2i}/\varepsilon)}, \tag{21a}$$

$$\frac{\partial g}{\partial \Im\{\boldsymbol{\theta}^H\}} = \sum_{i=1}^{K\Omega^K} \frac{\exp(f_{2i-1}/\varepsilon)\mathbf{b}_{2i-1}^T + \exp(f_{2i}/\varepsilon)\mathbf{b}_{2i}^T}{\exp(f_{2i-1}/\varepsilon) + \exp(f_{2i}/\varepsilon)}. \tag{21b}$$

Then, the Euclidean gradient can be readily calculated by substituting (20) and (21) into (19). The Riemannian gradient is thus given by

$$\mathrm{grad}_{\widetilde{\boldsymbol{\Theta}}} g = \mathcal{P}_{\widetilde{\boldsymbol{\Theta}}}\left(\nabla_{\widetilde{\boldsymbol{\Theta}}} g\right) = \nabla_{\widetilde{\boldsymbol{\Theta}}} g - \widetilde{\boldsymbol{\Theta}}\mathrm{diag}\left\{\widetilde{\boldsymbol{\Theta}}^T \nabla_{\widetilde{\boldsymbol{\Theta}}} g\right\}, \tag{22}$$

where $\mathcal{P}_{\widetilde{\boldsymbol{\Theta}}}(\cdot)$ denotes the projection onto the tangent space.

With the Riemannian gradient, the conjugate gradient algorithm can be employed on the Rienmannian space, and is referred to as the Riemannian conjugate gradient (RCG) algorithm. Considering the characteristics of the Riemannian space, this line search method works in a different way than the standard CG algorithm. In the p-th iteration of RCG, the search direction $\mathbf{d}_p$ is determined by the Riemannian gradient $\mathrm{grad}_{\widetilde{\boldsymbol{\Theta}}} g(\widetilde{\boldsymbol{\Theta}}_p)$ and the $(p-1)$-th search direction $\mathbf{d}_{p-1}$. Since these two vectors lie in different tangent spaces, they cannot be directly combined. Thus, the Riemannian transport operation is needed to map $\mathbf{d}_{p-1}$ into the tangent space of $\mathrm{grad}_{\widetilde{\boldsymbol{\Theta}}} g(\widetilde{\boldsymbol{\Theta}}_p)$. Then, the search direction $\mathbf{d}_p$ is given by

$$\mathbf{d}_p = -\mathrm{grad}_{\widetilde{\boldsymbol{\Theta}}} g(\widetilde{\boldsymbol{\Theta}}_p) + \beta_p \mathbf{d}_{p-1}^{\mathrm{t}}, \tag{23}$$

where β_p is the Polak-Ribiere parameter [48] and the superscript "t" indicates the Riemannian transport operation. The step size α_p is chosen by the Armijo backtracking line search method [48] and the p-th update is thus expressed as

$$\widetilde{\boldsymbol{\Theta}}_p = \mathrm{Retr}_{\widetilde{\boldsymbol{\Theta}}}\left(\widetilde{\boldsymbol{\Theta}}_{p-1} + \alpha_p \mathbf{d}_p\right), \tag{24}$$

where $\mathrm{Retr}_{\widetilde{\boldsymbol{\Theta}}}(\cdot)$ indicates the retraction operation, which maps the point on the tangent space to the manifold.

After obtaining $\widetilde{\boldsymbol{\Theta}}^*$, the optimal $\boldsymbol{\theta}^*$ can be constructed as

$$\boldsymbol{\theta}^* = [\widetilde{\boldsymbol{\Theta}}^*(1,:)]^T + j[\widetilde{\boldsymbol{\Theta}}^*(2,:)]^T. \tag{25}$$

The RCG algorithm to obtain $\boldsymbol{\theta}^*$ is summarized in Algorithm 1, where $N_{\max}$ is the maximum number of iterations and δ_{th} is the threshold to judge convergence.

In realistic IRS implementations, low-resolution digital phase shifters are more hardware-efficient and practical. A discrete phase-shift $\boldsymbol{\theta}_{\mathrm{d}}$ for the IRS using B bits of resolution can thus be calculated by direct quantization, i.e.,

$$\boldsymbol{\theta}_{\mathrm{d}}(n) = \mathrm{round}\left\{\frac{\boldsymbol{\theta}^*(n)}{2\pi/2^B}\right\} \times \frac{2\pi}{2^B}, \forall n, \tag{26}$$

where $\mathrm{round}\{\cdot\}$ indicates rounding to the nearest integer.

Now, with the previous developments, the joint symbol-level precoding and reflecting design for the power minimization problem is straightforward. Given an initial value $\boldsymbol{\theta}_0$, the symbol-level precoders $\mathbf{x}_m, m = 1, \ldots, \Omega^K$, and the IRS phase shifts $\boldsymbol{\theta}$ are iteratively updated by solving (7) and (8) until convergence is found. This joint symbol-level precoding and reflecting algorithm for the power minimization problem is summarized in Algorithm 2. Selection of an initial $\boldsymbol{\theta}_0$ will be addressed in Section V.

Algorithm 1 RCG-Based IRS Reflecting Design

Input: $g(\widetilde{\boldsymbol{\Theta}})$, $\widetilde{\boldsymbol{\Theta}}_0 \in \mathcal{M}$, $N_{\max}$, δ_{th}.
Output: $\boldsymbol{\theta}^*$.
1: Initialize $p = 0$, $\delta = \infty$, $\mathbf{d}_0 = -\mathrm{grad}_{\widetilde{\boldsymbol{\Theta}}} g(\widetilde{\boldsymbol{\Theta}}_0)$.
2: **while** $p \leq N_{\max}$ and $\delta \geq \delta_{\mathrm{th}}$ **do**
3: Calculate Riemannian gradient $\mathrm{grad}_{\widetilde{\boldsymbol{\Theta}}} g(\widetilde{\boldsymbol{\Theta}}_p)$ by (22).
4: Choose Polak-Ribiere parameter β_p [48].
5: Calculate search direction $\mathbf{d}_p$ by (23).
6: Calculate Armijo backtracking line search step size α_p [48].
7: Obtain $\widetilde{\boldsymbol{\Theta}}_p$ by (24).
8: $\delta = \left\|\mathrm{grad}_{\widetilde{\boldsymbol{\Theta}}} g(\widetilde{\boldsymbol{\Theta}}_p)\right\|^2$
9: $p = p + 1$.
10: **end while**
11: $\widetilde{\boldsymbol{\Theta}}^* = \widetilde{\boldsymbol{\Theta}}_p$.
12: Construct $\boldsymbol{\theta}^*$ by (25)

Algorithm 2 Joint Symbol-Level Precoding and Reflecting Design for the Power Minimization Problem

Input: $\mathbf{h}_k$, $\mathbf{h}_{rk}$, $\mathbf{G}$, Ω, σ_k, Γ_k, B, $N_{\max}$, δ_{th}.
Output: $\boldsymbol{\theta}^*$, $\mathbf{X}^*$.
1: Initialize $\boldsymbol{\theta}_0$ by solving (41), $iter = 0$, $\delta = \infty$, $p_{\mathrm{t}} = 0$.
2: **while** $iter \leq N_{\max}$ and $\delta \geq \delta_{\mathrm{th}}$ **do**
3: $p_{\mathrm{pre}} = p_{\mathrm{t}}$.
4: Calculate precoder $\mathbf{x}_m, m = 1, \ldots, \Omega^K$, by (7).
5: Obtain infinite resolution IRS phase shifts $\boldsymbol{\theta}$ using Algorithm 1.
6: Calculate $\boldsymbol{\theta}_{\mathrm{d}}$ by (26) for the low-resolution IRS phase shifts cases.
7: $p_{\mathrm{t}} = \|\mathbf{X}\|_F^2$.
8: $\delta = \left|\frac{p_{\mathrm{t}} - p_{\mathrm{re}}}{p_{\mathrm{re}}}\right|$.
9: $iter = iter + 1$.
10: **end while**
11: $\boldsymbol{\theta}^* = \boldsymbol{\theta}$ or $\boldsymbol{\theta}_{\mathrm{d}}$, $\mathbf{X}^* = \mathbf{X}$.

IV. Algorithm for QoS Balancing Problem

In this section, we first formulate the QoS balancing problem for the considered IRS-enhanced MU-MISO system. Then, a similar algorithm is proposed to iteratively solve the symbol-level precoding and reflecting design problems.

As discussed in Section II, the distance between the received noise-free signal and its decision boundaries essentially determines symbol detection performance; larger distances provide stronger robustness against noise, and thus a lower SER. Therefore, we use this distance as the QoS metric and aim at maximizing the minimum QoS among the users with a given power budget. From Fig. 2, we observe that the distance between point D and its decision boundaries (i.e., the positive

halves of the x and y axes in this case) can be expressed as

$$\begin{aligned}&\left|\overrightarrow{D'E}\right| \\ &= \left|\overrightarrow{D'F}\right|\cos\Phi = \left(\left|\overrightarrow{B'F}\right| - \left|\overrightarrow{B'D'}\right|\right)\cos\Phi \\ &= \left[\Re\{\widetilde{r}_{m,k}e^{-j\angle s_{m,k}}\}\tan\Phi - \left|\Im\{\widetilde{r}_{m,k}e^{-j\angle s_{m,k}}\}\right|\right]\cos\Phi.\end{aligned} \tag{27}$$

Thus, after ignoring the constant term $\cos\Phi$, the QoS balancing problem can be formulated as

$$\max_{\mathbf{X},\boldsymbol{\theta}} \min_{m,k} \Re\left\{\widetilde{r}_{m,k}e^{-j\angle s_{m,k}}\right\}\tan\Phi - \left|\Im\left\{\widetilde{r}_{m,k}e^{-j\angle s_{m,k}}\right\}\right| \tag{28a}$$

$$\text{s.t. } \widetilde{r}_{m,k} = \left(\mathbf{h}_k^H + \mathbf{h}_{\mathrm{r}k}^H\boldsymbol{\Theta}\mathbf{G}\right)\mathbf{x}_m, \quad \forall k,\forall m, \tag{28b}$$

$$\boldsymbol{\Theta} = \mathrm{diag}\{\boldsymbol{\theta}\}, |\theta_n| = 1, \quad \forall n, \tag{28c}$$

$$\|\mathbf{X}\|^2 \le P\Omega^K, \tag{28d}$$

where P is the preset average transmit power budget. As before, we propose to decompose this bivariate problem into separate symbol-level precoding design and the reflecting design problems, and solve them iteratively.

A. Symbol-Level Precoding Design for QoS Balancing Problem

With given IRS phase shifts $\boldsymbol{\theta}$, the combined channel vector from the BS to the k-th user is $\widetilde{\mathbf{h}}_k^H \triangleq \mathbf{h}_k^H + \mathbf{h}_{\mathrm{r}k}^H\boldsymbol{\Theta}\mathbf{G}$. Then, the QoS balancing problem for designing the precoder $\mathbf{X}$ can be rewritten as

$$\max_{\mathbf{X},t} t \tag{29a}$$

$$\begin{aligned}\text{s.t. } &\Re\{\widetilde{\mathbf{h}}_k^H\mathbf{x}_m e^{-j\angle s_{m,k}}\}\tan\Phi \\ &- \left|\Im\{\widetilde{\mathbf{h}}_k^H\mathbf{x}_m e^{-j\angle s_{m,k}}\}\right| \ge t, \quad \forall k,\forall m,\end{aligned} \tag{29b}$$

$$\|\mathbf{X}\|^2 \le P\Omega^K, \tag{29c}$$

which is a convex problem and can be solved by standard convex optimization tools, e.g., CVX. However, since the variable to be optimized $\mathbf{X}$ has a large dimension of $M\Omega^K$, the complexity is unaffordable. In order to deal with this difficulty, we decompose this problem into Ω^K sub-problems, where $\mathbf{x}_m, \forall m$, is individually designed. To facilitate the algorithm development, we propose the following proposition.

Proposition 1: Let $\mathbf{x}_1^*,\ldots,\mathbf{x}_{\Omega^K}^*$ be the optimal solution of the QoS balancing problem (29). Let $\mathbf{x}_1^\star,\ldots,\mathbf{x}_{\Omega^K}^\star$ be the optimal solution of the power minimization problem (7), where the QoS requirement for all users equals $t_0 = \sigma_k\sqrt{\Gamma_k}\tan\Phi, \forall k$. Then, $\mathbf{x}_m^*$ is a scaled version of $\mathbf{x}_m^\star$, i.e., $\mathbf{x}_m^* = \frac{\sqrt{P_m}\mathbf{x}_m^\star}{\|\mathbf{x}_m^\star\|}$, where $P_m \ge 0$ is the transmit power allocated to the m-th precoder, $\sum_{m=1}^{\Omega^K} P_m = P\Omega^K$. Furthermore, the minimum QoS that $\mathbf{x}_m^*$ can achieve is $\frac{\sqrt{P_m}t_0}{\|\mathbf{x}_m^\star\|}$.

Proof: See Appendix. ∎

Proposition 1 indicates that we can first find the precoder $\mathbf{x}_m^\star$ by individually solving the power minimization problem (7) with a given QoS requirement t_0, and then scaling $\mathbf{x}_m^\star$ appropriately to obtain the optimal $\mathbf{x}_m^*$ by finding the optimal power allocation P_m. With given $\mathbf{x}_m^\star$, the power allocation problem to optimize QoS balancing can be formulated as

$$\max_{P_m,\forall m} t \tag{30a}$$

$$\text{s.t. } t \le \frac{\sqrt{P_m}t_0}{\|\mathbf{x}_m^\star\|}, \quad \forall m, \tag{30b}$$

$$\sum_{m=1}^{\Omega^K} P_m \le P\Omega^K. \tag{30c}$$

While (30) is convex and can be solved by CVX, we attempt to find a more efficient solution to reduce the complexity. Denoting $\mathbf{p} \triangleq \left[\sqrt{P_1},\ldots,\sqrt{P_{\Omega^K}}\right]^T$, the power allocation problem (30) can be rewritten as

$$\max_{\mathbf{p},t} t \tag{31a}$$

$$\text{s.t. } t \le \mathbf{e}_m^T\mathbf{p}, \quad \forall m, \tag{31b}$$

$$\|\mathbf{p}\|^2 \le P\Omega^K, \tag{31c}$$

where $\mathbf{e}_m$ is a vector of all zeros except the m-th element which is $\frac{t_0}{\|\mathbf{x}_m^\star\|}$. Motivated by Proposition 1, we first find $\mathbf{p}^\star$, which is the optimal solution for the following power minimization problem with an arbitrary given $t_0' \ge 0$:

$$\min_{\mathbf{p}} \|\mathbf{p}\|^2 \tag{32a}$$

$$\text{s.t. } \mathbf{e}_m^T\mathbf{p} \ge t_0', \quad \forall m. \tag{32b}$$

This problem can be efficiently solved using the same method as in problem (7), based on the Lagrangian dual problem and exploiting the gradient projection algorithm. Then, the optimal $\mathbf{p}^*$ for (31) can be obtained by $\mathbf{p}^* = \frac{\sqrt{P\Omega^K}\mathbf{p}^\star}{\|\mathbf{p}^\star\|}$.

With the above analysis, the symbol-level precoding algorithm for the QoS balancing problem can be summarized as: *i*) obtain the precoder $\mathbf{x}_m^\star$ by solving the power minimization problem (7) with a certain QoS requirement $t_0 \ge 0$; *ii*) solving the power allocation problem (30) to obtain $P_m, \forall m$; *iii*) scaling $\mathbf{x}_m^\star$ to obtain the optimal solution of (29) as $\mathbf{x}_m^* = \frac{\sqrt{P_m}\mathbf{x}_m^\star}{\|\mathbf{x}_m^\star\|}$.

B. Reflecting Design for QoS Balancing Problem

With fixed precoders $\mathbf{x}_1,\ldots,\mathbf{x}_{\Omega^K}$, the reflecting design problem is given by

$$\max_{\boldsymbol{\theta}} \min_{m,k} \Re\{\widetilde{r}_{m,k}e^{-j\angle s_{m,k}}\}\tan\Phi - \left|\Im\{\widetilde{r}_{m,k}e^{-j\angle s_{m,k}}\}\right| \tag{33a}$$

$$\text{s.t. } \widetilde{r}_{m,k} = \left(\mathbf{h}_k^H + \mathbf{h}_{\mathrm{r}k}^H\boldsymbol{\Theta}\mathbf{G}\right)\mathbf{x}_m, \quad \forall k,\forall m, \tag{33b}$$

$$\boldsymbol{\Theta} = \mathrm{diag}\{\boldsymbol{\theta}\}, |\theta_n| = 1, \quad \forall n. \tag{33c}$$

Using the definitions in (9), the reflecting design problem is more compactly formulated as

$$\min_{\boldsymbol{\theta}} \max_{m,k} \left|\Im\left\{\widehat{r}_{m,k}\right\}\right| - \Re\left\{\widehat{r}_{m,k}\right\}\tan\Phi \tag{34a}$$

$$\text{s.t. } |\theta_n| = 1, \quad \forall n. \tag{34b}$$

As before, (34a) is non-differentiable due to the max and absolute value functions and (34b) is non-convex, which leads us to exploit the RCG algorithm. To facilitate the RCG

algorithm, the same idea used to solve (10a) is employed here in three steps: *i*) replacing the absolute value function, *ii*) smoothing the max function, *iii*) calculating its Euclidean gradient. We briefly describe these three steps below.

The absolute value function is replaced using (11), and the problem is further rearranged as

$$\min_{\widetilde{\boldsymbol{\Theta}}} \max_{i} \ f_i \tag{35a}$$

$$\text{s.t. } [\widetilde{\boldsymbol{\Theta}}(:,n)]^T \widetilde{\boldsymbol{\Theta}}(:,n) = 1, \quad \forall n, \tag{35b}$$

where f_i is defined in (14) with the auxiliary vectors $\mathbf{a}_{2i-1}$, $\mathbf{b}_{2i-1}$, $\mathbf{a}_{2i}$ $\mathbf{b}_{2i}$ in (15a), (15b), (15d), (15e), and

$$c_{2i-1} \triangleq \Im\{a_{m,k}\} - \Re\{a_{m,k}\} \tan \Phi, \tag{36a}$$

$$c_{2i} \triangleq -\Im\{a_{m,k}\} - \Re\{a_{m,k}\} \tan \Phi. \tag{36b}$$

We smooth the max function by exploiting the log-sum-exp algorithm, which introduces the approximation

$$\begin{aligned} \max\{f_1, f_2, \ldots, f_{2\Omega^K}\} &\approx g(\widetilde{\boldsymbol{\Theta}}) \\ &\triangleq \varepsilon \log \left\{ \sum_{i=1}^{K\Omega^K} \left[\exp\left(\frac{f_{2i-1}}{\varepsilon}\right) + \exp\left(\frac{f_{2i}}{\varepsilon}\right) \right] \right\}, \end{aligned} \tag{37}$$

where ε is a small positive number.

After obtaining the smooth and differentiable $g(\widetilde{\boldsymbol{\Theta}})$, its Euclidean gradient can be derived by substituting (20) into (19), where we need to calculate

$$\frac{\partial g}{\partial \Re\{\boldsymbol{\theta}^H\}} = \frac{\sum_{i=1}^{K\Omega^K} \left[\exp(f_{2i-1}/\varepsilon)\mathbf{a}_{2i-1}^T + \exp(f_{2i}/\varepsilon)\mathbf{a}_{2i}^T\right]}{\sum_{i=1}^{K\Omega^K} \left[\exp(f_{2i-1}/\varepsilon) + \exp(f_{2i+1}/\varepsilon)\right]}, \tag{38a}$$

$$\frac{\partial g}{\partial \Im\{\boldsymbol{\theta}^H\}} = \frac{\sum_{i=1}^{K\Omega^K} \left[\exp(f_{2i-1}/\varepsilon)\mathbf{b}_{2i-1}^T + \exp(f_{2i}/\varepsilon)\mathbf{b}_{2i}^T\right]}{\sum_{i=1}^{K\Omega^K} \left[\exp(f_{2i-1}/\varepsilon) + \exp(f_{2i+1}/\varepsilon)\right]}. \tag{38b}$$

Then, the RCG-based reflecting design in Algorithm 1 can be applied to solve the QoS balancing problem. The optimal IRS phase shifts $\boldsymbol{\theta}^*$ and low-resolution phase shifts $\boldsymbol{\theta}_{\rm d}$ have the same format as in (25) and (26).

Finally, the joint symbol-level precoding and reflecting design for the QoS balancing problem is straightforward. With an initial reflecting value $\boldsymbol{\theta}_0$, the symbol-level precoding matrix $\mathbf{X}$ and the IRS phase shifts $\boldsymbol{\theta}$ are iteratively updated by solving (29) and (33) until convergence is found.

V. Initialization and Complexity Analysis

A. Initialization

Since the RCG algorithm in general will find a locally optimal solution, an initial value that is close to the optimal solution can provide better performance and accelerate convergence. In this subsection, we propose a heuristic method to obtain the initial $\boldsymbol{\theta}_0$.

Both the power minimization and QoS balancing problems depend on the quality of the users' channels, which can be manipulated by the IRS. Therefore, without considering the precoding, we can simply design the IRS phase shifts to maximize the minimum channel gain for all users:

$$\max_{\boldsymbol{\theta}_0} \min_{k} \ \left\|\mathbf{h}_k^H + \mathbf{h}_{{\rm r}k}^H \boldsymbol{\Theta}_0 \mathbf{G}\right\|^2 \tag{39a}$$

$$\text{s.t. } \boldsymbol{\Theta}_0 = \text{diag}\{\boldsymbol{\theta}_0\}, |\theta_n| = 1, \quad \forall n. \tag{39b}$$

For the algorithm development, we rewrite the objective function (39a) in a more concise format as

$$\begin{aligned} f_k(\boldsymbol{\theta}_0) &\triangleq \left\|\mathbf{h}_k^H + \mathbf{h}_{{\rm r}k}^H \boldsymbol{\Theta}_0 \mathbf{G}\right\|^2 = \left\|\mathbf{h}_k^H + \boldsymbol{\theta}_0^H \mathbf{G}_k\right\|^2 \\ &= \boldsymbol{\theta}_0^H \mathbf{G}_k \mathbf{G}_k^H \boldsymbol{\theta}_0 + \boldsymbol{\theta}_0^H \mathbf{G}_k \mathbf{h}_k + \mathbf{h}_k^H \mathbf{G}_k^H \boldsymbol{\theta}_0 + \mathbf{h}_k^H \mathbf{h}_k, \end{aligned} \tag{40}$$

where $\mathbf{G}_k \triangleq \text{diag}\left\{\mathbf{h}_{{\rm r}k}^H\right\} \mathbf{G}, \forall k$, for simplicity. Then, using the log-sum-exp approximation, problem (39) is reformulated as

$$\min_{\boldsymbol{\theta}_0} \ g(\boldsymbol{\theta}_0) \triangleq \varepsilon \log \sum_{k=1}^{K} \exp\left[\frac{-f_k(\boldsymbol{\theta}_0)}{\varepsilon}\right] \tag{41a}$$

$$\text{s.t. } |\theta_n| = 1, \quad \forall n, \tag{41b}$$

where the unit modulus constraint (41b) forms an N-dimensional complex circle manifold

$$\mathcal{M} = \left\{\boldsymbol{\theta}_0 \in \mathbb{C}^N : |\theta_n| = 1, \forall n\right\}, \tag{42}$$

with the tangent space

$$T_{\boldsymbol{\theta}_0}\mathcal{M} = \left\{\mathbf{p} \in \mathbb{C}^N : \Re\left\{\mathbf{p} \circ \boldsymbol{\theta}_0^*\right\} = \mathbf{0}_N\right\}. \tag{43}$$

The Riemannian gradient of $g(\boldsymbol{\theta}_0)$ is thus given by

$$\text{grad}_{\boldsymbol{\theta}_0} g = \bigtriangledown_{\boldsymbol{\theta}_0} g - \Re\left\{\bigtriangledown_{\boldsymbol{\theta}_0} g \circ \boldsymbol{\theta}_0^*\right\} \circ \boldsymbol{\theta}_0, \tag{44}$$

where the Euclidean gradient $\bigtriangledown_{\boldsymbol{\theta}_0} g$ can be calculated as

$$\bigtriangledown_{\boldsymbol{\theta}_0} g = \frac{\sum_{k=1}^{K} \left\{\exp\left[\frac{-f_k(\boldsymbol{\theta}_0)}{\varepsilon}\right] \left(-2\mathbf{G}_k \mathbf{G}_k^H \boldsymbol{\theta}_0 - 2\mathbf{G}_k \mathbf{h}_k\right)\right\}}{\sum_{k=1}^{K} \exp\left[\frac{-f_k(\boldsymbol{\theta}_0)}{\varepsilon}\right]}. \tag{45}$$

Then, following the same procedure as in Algorithm 1, the initialization $\boldsymbol{\theta}_0$ can be easily obtained.

B. Complexity Analysis

In this subsection, we provide a brief complexity analysis for the proposed joint symbol-level precoding and reflecting design algorithms. The complexity to obtain the initial $\boldsymbol{\theta}_0$ is at most $\mathcal{O}\{N^{1.5}\}$ using the RCG algorithm. For the power minimization problem, the complexity to solve for the precoder $\mathbf{x}_m$ by the gradient projection algorithm is $\mathcal{O}\{M^3\}$, and the worst-case computation for the RCG algorithm is of order $\mathcal{O}\{(2N)^{1.5}\}$. Therefore, the total computational complexity of Algorithm 2 is $\mathcal{O}\{\Omega^K M^3 + (2N)^{1.5}\}$. The symbol-level precoding algorithm for the QoS balancing problem is derived by solving the corresponding power minimization problem, and the reflecting designs for these two problems are similar. Thus, the complexity to solve the QoS balancing problem is the same as the power minimization problem.

For comparison, the complexity of the joint linear block-level precoding and reflecting design in [10] should also be analyzed. In [10], the linear block-level precoding design is a second-order cone program (SOCP) problem with a

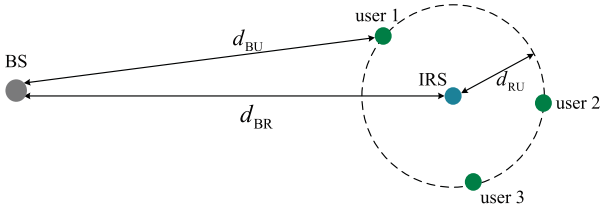

Fig. 3. Simulation setup for multiuser case.

complexity of order $\mathcal{O}\left\{M^{4.5}K^{3.5}\right\}$, and the reflecting design is solved using a semidefinite relaxation (SDR) algorithm, whose complexity is of order $\mathcal{O}\left\{K^{3.5}N^{2.5}+K^{2.5}N^{3.5}\right\}$. Therefore, the total complexity of the proposed algorithm in [10] is of order $\mathcal{O}\left\{M^{4.5}K^{3.5}+K^{3.5}N^{2.5}+K^{2.5}N^{3.5}\right\}$. We can observe that the algorithm in [10] has polynomial complexity in the number of transmit antennas, reflecting elements and users, while the proposed algorithm has exponential complexity in the number of users and the base is the order of the modulation. However, the significant performance gains obtained by the proposed approach make it worth considering despite the resulting complexity; in cases where the number of users or the modulation order are not very large, the required computational load is still manageable.

VI. Simulation Results

In this section, we provide extensive simulation results to illustrate the effectiveness of our proposed algorithms. For simplicity, we assume either QPSK ($\Omega = 4$) or 8-PSK modulation ($\Omega = 8$) are used. The QoS requirement and the noise power for $K = 3$ users is the same, i.e., $\Gamma = \Gamma_k, \forall k, \sigma^2 = \sigma_k^2 = -80$dBm, $\forall k$. The transmit antenna array at the BS is assumed to be a uniform linear array with antenna spacing given by $\lambda/2$. The distance-dependent path loss is modeled as $\mathrm{PL}(d) = C_0\left(\frac{d}{d_0}\right)^{-\alpha}$, where $C_0 = -30$dB is the path loss for the reference distance $d_0 = 1$m, d is the link distance, and α is the path-loss exponent. In addition, the small-scale Rician fading channel model for all channels is assumed, which consists of line-of-sight (LoS) and non-LoS (NLoS) components. The channels from the BS to the IRS can be expressed as

$$\mathbf{G} = \sqrt{\frac{\kappa}{\kappa+1}}\mathbf{G}^{\mathrm{LoS}} + \sqrt{\frac{1}{\kappa+1}}\mathbf{G}^{\mathrm{NLoS}}, \tag{46}$$

where κ is the Rician factor set as 3dB, $\mathbf{G}^{\mathrm{LoS}}$ is the LoS component which depends on the geometric settings, and $\mathbf{G}^{\mathrm{NLoS}}$ is the NLoS Rayleigh fading component. The MISO channels $\mathbf{h}_k$ and $\mathbf{h}_{\mathrm{r}k}, k = 1, \ldots, K$, are assumed to obey a similar model, consisting of LoS and NLoS components.

The geometry of the following simulations is shown in Fig. 3, from a top-down view. The IRS is typically deployed close to the users to provide them with performance gains, since they may suffer from blockage and severe attenuation. Therefore, we set the distance between the BS and the IRS as $d_{\mathrm{BR}} = 50$m, the distance between the IRS and the users as $d_{\mathrm{RU}} = 3$m, and the distance between the BS and each user as d_{BU}, which lies in the interval $[d_{\mathrm{BR}} - d_{\mathrm{RU}}, d_{\mathrm{BR}} + d_{\mathrm{RU}}]$. The users are randomly distributed on the dashed circle in Fig. 3. Considering the link distance, the path-loss exponents for $\mathbf{h}_k$, $\mathbf{h}_{\mathrm{r}k}$ and $\mathbf{G}$ are set as 3.5, 2.8, and 2.5, respectively. Similar settings are widely adopted in existing works, e.g., [10].

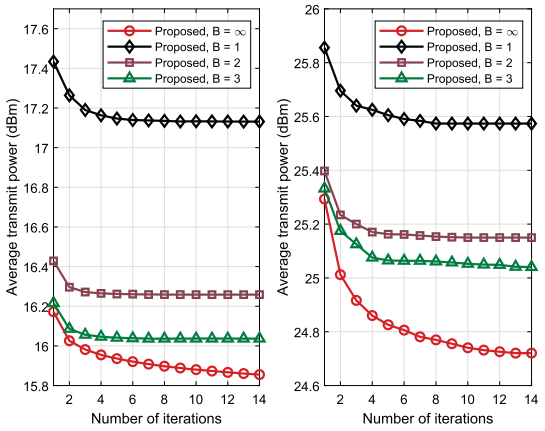

(a) QPSK (b) 8-PSK

Fig. 4. Average transmit power versus the number of iterations ($K = 3$ users, $N = 64$ reflecting elements, $M = 6$ transmit antennas, $\Gamma = 10$ dB).

A. Power Minimization Problem

In this subsection, we illustrate the simulation results for the power minimization problem. We first show in Fig. 4 the convergence of our proposed algorithm for the cases where the IRS has continuous, 1-bit, 2-bit, and 3-bit phase shifters, i.e., $B = \infty, 1, 2, 3$, respectively. It can be observed that our proposed algorithm converges within 14 iterations for all schemes and the low-resolution cases have much faster convergence. We also see that the QPSK case converges more quickly than the 8-PSK case and achieves a lower transmit power, but there is a relatively large gap between the continuous and low-resolution cases. These convergence results are encouraging for a low-complexity implementation.

In Fig. 5, we show the average transmit power versus the QoS requirement Γ. In order to demonstrate the effectiveness of our proposed joint symbol-level precoding and reflecting design, we also include: *i*) Symbol-level precoding without the aid of the IRS (denoted as "SLP, w/o IRS"); *ii*) linear block-level precoding with the aid of IRS and continuous phase shifters [10] (denoted as "BLP, w/ IRS, $B = \infty$"); *iii*) linear block-level precoding without the aid of the IRS [49] (denoted as "BLP, w/o IRS"). It can be seen from Fig. 5 that our proposed scheme requires less transmit power than the "SLP, w/o IRS" approach in both the QPSK and 8-PSK cases, which validates the effectiveness of using IRS in the symbol-level precoding systems. We can also observe that the proposed joint symbol-level precoding and reflecting algorithm outperforms the "BLP, w/ IRS, $B = \infty$" and "BLP, w/o IRS" approaches, which verifies the performance improvement due to symbol-level precoding. In addition, it is noted that with increasing B, better system performance can be achieved. Moreover, the 3-bit quantized solution can provide

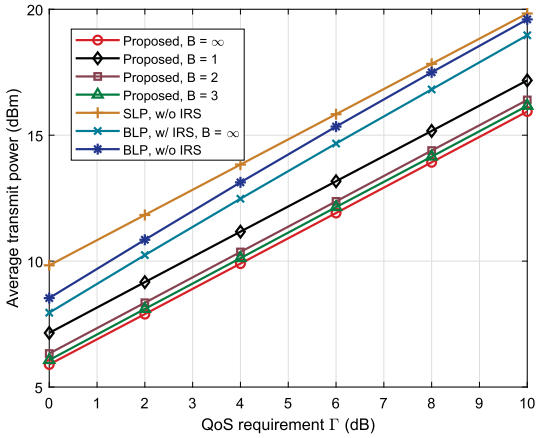

(a) QPSK

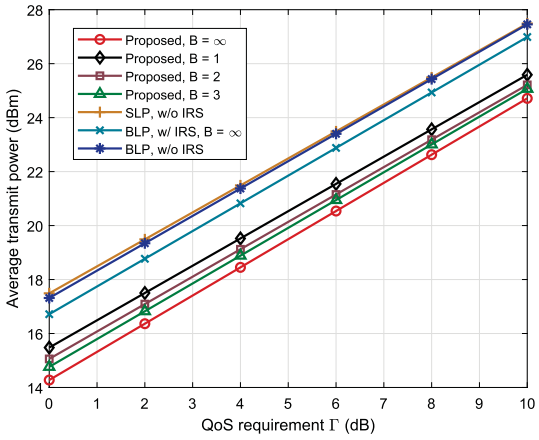

(b) 8-PSK

Fig. 5. Average transmit power versus QoS requirement Γ ($K = 3$ users, $N = 64$ reflecting elements, $M = 6$ transmit antennas).

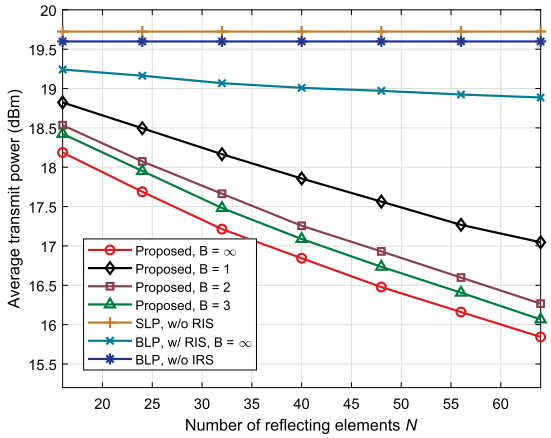

Fig. 6. Average transmit power versus the number of reflecting elements N ($K = 3$ users, $M = 6$ transmit antennas, $\Gamma = 10$ dB).

performance similar to the ideal unquantized solution, thus providing a favorable trade-off between cost and performance. Beyond $B = 3$ bits, the extra cost and complexity associated with using higher-resolution IRS are not warranted given the very marginal increase in system performance. On the other hand, the performance gap between the different approaches in Fig. 5(b) is relatively smaller than that in Fig. 5(a), which indicates that higher-order modulation can compensate for the performance loss due to low-resolution phase shifts or non-optimal precoders. However, significantly more transmit power is required to support higher-order modulation.

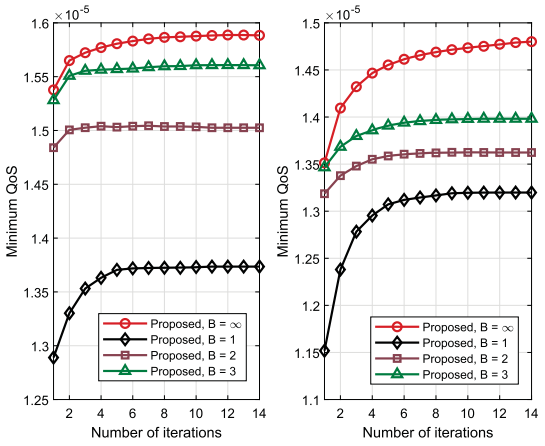

Fig. 7. Minimum QoS versus the number of iterations ($K = 3$ users, $N = 64$ reflecting elements, $M = 6$ transmit antennas, $P = 20$ dBm).

Next, we focus on QPSK modulation and present the average transmit power versus the number of reflecting elements N in Fig. 6. The same relationship can be observed as in Fig. 5. We observe that as the number of reflecting elements increases, the average transmit power is greatly reduced, and the reduction is more pronounced for our proposed SLP algorithms compared with linear block-level precoding. This supports the main idea of our paper, that the combination of SLP and IRS provides symbiotic benefits.

B. QoS Balancing Problem

In this subsection, we present simulations for the QoS balancing problem. The convergence performance is similar to that observed for the power minimization problem in Fig. 7. It is seen that all schemes converges within 14 iterations, which indicates favorable computational complexity.

In Fig. 8, we plot the worst-case performance t achieved for the QoS balancing problem versus the transmit power P. As the transmit power increases, the minimum QoS of all methods increases, which means that the distance between the received noise-free signal and its decision boundaries becomes larger. The minimum QoS achieved by our proposed joint symbol-level precoding and reflecting algorithm is dramatically larger than the other competitors, which further supports the benefit of using IRS together with symbol-level precoding.

In order to demonstrate the QoS improvement in a more intuitive and natural way with a familiar metric, in Fig. 9 we present the average SER versus the transmit power. Obviously, the larger QoS requirement (i.e., Γ), which results in a larger distance between the received signal and its decision boundaries, leads to better performance in terms of a lower SER. This relationship can be verified by comparing Figs. 8 and 9. More importantly, the improvement in the

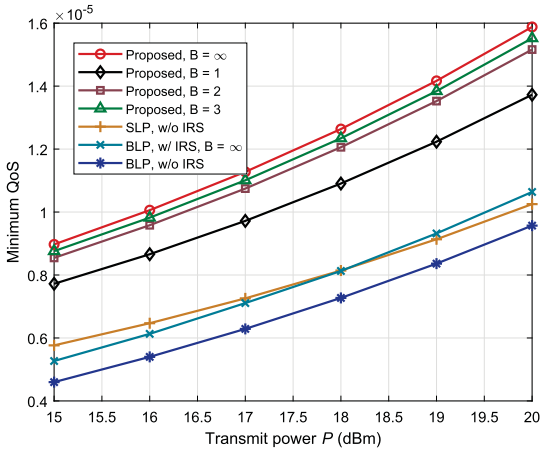

(a) QPSK

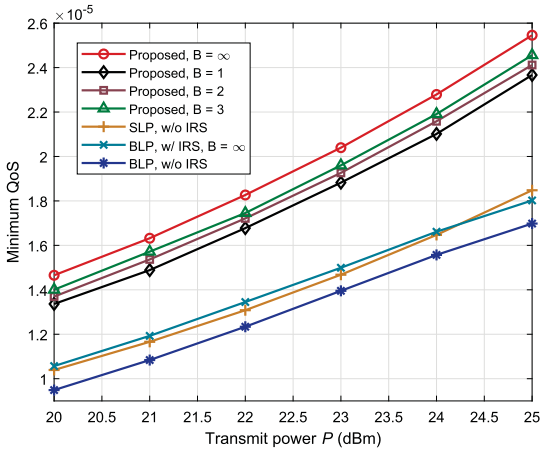

(b) 8-PSK

Fig. 8. Minimum QoS versus the transmit power P ($K = 3$ users, $N = 64$ reflecting elements, $M = 6$ transmit antennas).

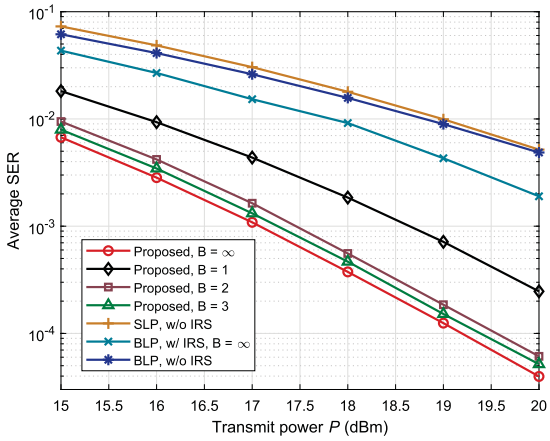

(a) QPSK

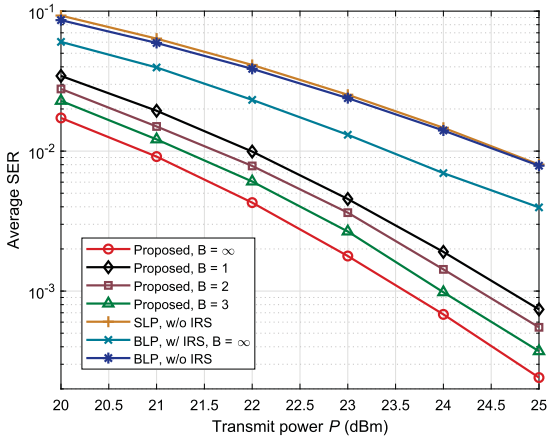

(b) 8-PSK

Fig. 9. Average SER versus the transmit power P ($K = 3$ users, $N = 64$ reflecting elements, $M = 6$ transmit antennas).

SER performance of our proposed algorithm is also very remarkable. When the 3-bit IRS can offer close to 10^{-4} SER, the symbol-level precoding system without IRS provides only 10^{-2} SER. Therefore, utilizing the QoS requirement Γ as the performance metric for optimizing the IRS-enhanced symbol-level precoding systems is reasonable and effective.

Next, we show the average SER versus the number of reflecting elements N for QPSK modulation in Fig. 10. Since the larger IRS can provide larger beamforming/reflecting gains, we observe that the average SER decreases for all schemes with increasing N. Moreover, our proposed schemes always achieve significantly better SER performance for different IRS sizes.

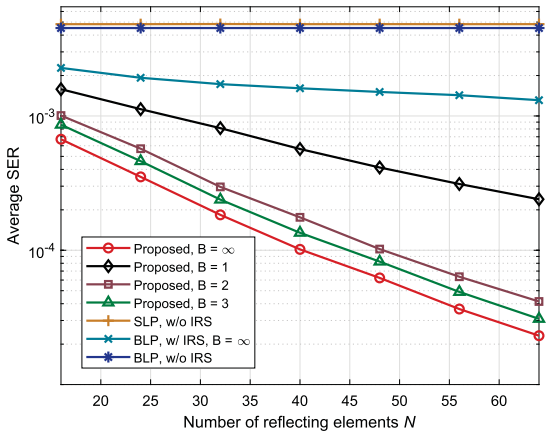

Fig. 10. Average SER versus the number of reflecting elements N ($K = 3$ users, $N = 64$ reflecting elements, $M = 6$ transmit antennas, $P = 20$ dBm).

C. Impact of IRS Location

In order to demonstrate the impact of IRS location, we focus on QPSK modulation and simulate a case where the position of one of the users changes along a horizontal line parallel to the line between the BS and IRS. As shown in Fig. 11, user 3 moves along the dashed line and the vertical distance between it and the BS-IRS link is $d_{\mathrm{v}} = 0.5$m. Let d_{m} be the horizontal distance between the BS and user 3. The other two users are still located 3m from the IRS. In Figs. 12 and 13, we show the system performance as a function of d_{m}. We observe that the proposed schemes always outperform other benchmarks, and the best performance is achieved when the user moves closest to the IRS, i.e., $d_{\mathrm{m}} = 50$m, since a larger reflection gain is obtained when the user is closest to the

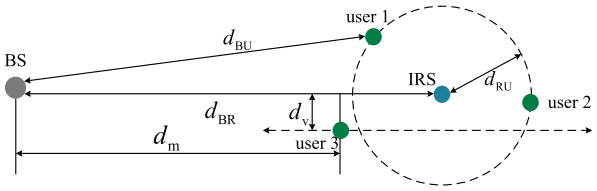

Fig. 11. Simulation setup for mobile user case.

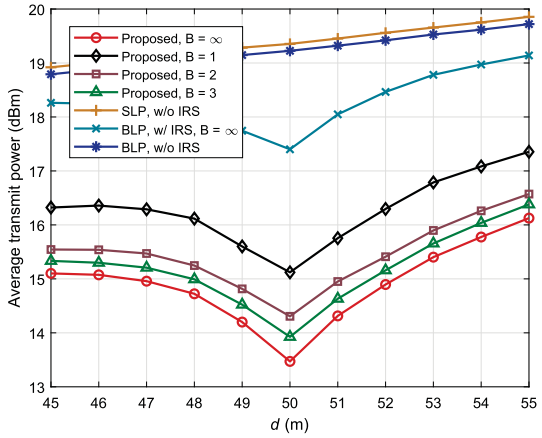

Fig. 12. Average transmit power versus d_{m} ($K = 3$ users, $N = 64$ reflecting elements, $M = 6$ transmit antennas, SNR $= 10$ dB).

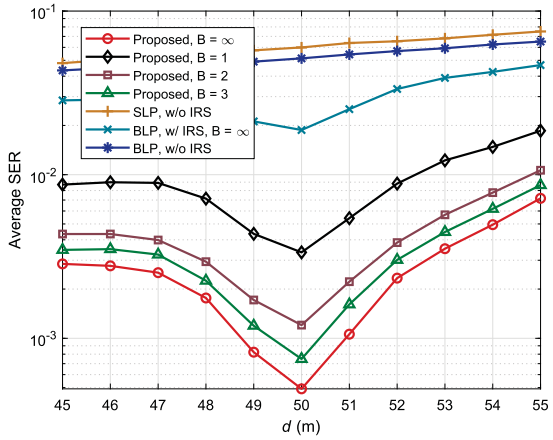

Fig. 13. Average SER versus d_{m} ($K = 3$ users, $N = 64$ reflecting elements, $M = 6$ transmit antennas, $P = 15$ dBm).

IRS. Moreover, when the users move closer together, MUI may become stronger, which can be effectively exploited by symbol-level precoding.

VII. Conclusion

In this article, we investigated IRS-enhanced wireless networks, where an IRS is deployed to assist the multi-user MISO communication system, which employs symbol-level precoding to exploit the multi-user interference. In particular, we considered the joint symbol-level precoding and reflecting design problems for IRS-enhanced MU-MISO systems. Efficient iterative algorithms were proposed to solve the power minimization and QoS balancing problems. The gradient-projection-based and Riemannian conjugate gradient (RCG)-based algorithms were used to design the symbol-level precoding and IRS phase shifts, respectively. The simulation results illustrated that our proposed algorithms exhibit remarkably better performance in terms of power-savings and SER-reductions. These positive results have confirmed that the employment of IRS in symbol-level precoding systems can provide more efficient multi-user interference exploitation by intelligently manipulating the multi-user channels.

Appendix

Proof: [Proof of Proposition 1] We assume the optimal solution of the QoS balancing problem (29) is $\mathbf{x}_m^*, \forall m$, and t^*, and we denote the transmit power allocated to the m-th precoder as $P_m \triangleq \|\mathbf{x}_m^*\|^2$. If the power allocations $P_m, \forall m$, are known, the QoS balancing problem can be divided into Ω^K sub-problems and the m-th sub-problem is written as

$$\max_{\mathbf{x}_m, t_m} \ t_m \tag{47a}$$

$$\text{s.t. } \Re\{\widetilde{\mathbf{h}}_k^H \mathbf{x}_m e^{-j\angle s_{m,k}}\} \tan\Phi - \left|\Im\{\widetilde{\mathbf{h}}_k^H \mathbf{x}_m e^{-j\angle s_{m,k}}\}\right| \geq t_m, \forall k, \tag{47b}$$

$$\|\mathbf{x}_m\|^2 \leq P_m. \tag{47c}$$

It can be easily verified that the inequality constraint (47c) holds with equality at the optimal $\mathbf{x}_m^*$. Moreover, $\mathbf{x}_m^*$ is also the optimal solution for the following power minimization problem:

$$\min_{\mathbf{x}_m} \ \|\mathbf{x}_m\|^2 \tag{48a}$$

$$\text{s.t. } \Re\{\widetilde{\mathbf{h}}_k^H \mathbf{x}_m e^{-j\angle s_{m,k}}\} \tan\Phi - \left|\Im\{\widetilde{\mathbf{h}}_k^H \mathbf{x}_m e^{-j\angle s_{m,k}}\}\right| \geq t_m^*, \quad \forall k. \tag{48b}$$

To prove this statement by contradiction, we start by assuming that $\mathbf{x}_m^*$ is not optimal for (48) and there exists another $\overline{\mathbf{x}}_m$ satisfying (48b) and requiring less power, i.e., $\|\overline{\mathbf{x}}_m\| < P_m$. Then, we can scale up $\overline{\mathbf{x}}_m$ to let the power constraint (47c) become equal and provide a higher t_m in (47), in which case $\mathbf{x}_m^*$ is not optimal any more, and this results in a contradiction.

If we use an arbitrary $t_0 > 0$ as the QoS requirement in (48b) instead of t_m^*, the optimal solution $\mathbf{x}_m^\star$ of this power minimization problem is the scaled version of $\mathbf{x}_m^*$, since the constraint (48b) is a linear function. More specifically, $\mathbf{x}_m^* = \frac{\sqrt{P_m}\mathbf{x}_m^\star}{\|\mathbf{x}_m^\star\|}$ with the optimal power P_m.

If we set the QoS requirement as $t_0 = \sigma_k\sqrt{\Gamma_k}\tan\Phi$, then (48) has the same format as (7), which implies that the optimal $\mathbf{x}_m^\star$ for the power minimization problem (7) is also a scaled version of the optimal $\mathbf{x}_m^*$ for the QoS balancing problem (29). Proposition 1 is therefore proved. ■

References

[1] R. Liu, H. Li, M. Li, and Q. Liu, "Symbol-level precoding design for IRS-assisted MU-MISO systems," in *Proc. IEEE Wireless Commun. Netw. Conf. (WCNC)*, Seoul, South Korea, May 2020, pp. 1–6.

[2] S. Zhang, Q. Wu, S. Xu, and G. Y. Li, "Fundamental green tradeoffs: Progresses, challenges, and impacts on 5G networks," *IEEE Commun. Surveys Tuts.*, vol. 19, no. 1, pp. 33–56, 1st Quart., 2017.

[3] A. L. Swindlehurst, E. Ayanoglu, P. Heydari, and F. Capolino, "Millimeter-wave massive MIMO: The next wireless revolution?" *IEEE Commun. Mag.*, vol. 52, no. 9, pp. 56–62, Sep. 2014.

[4] C. Liaskos, S. Nie, A. Tsioliaridou, A. Pitsillides, S. Ioannidis, and I. Akyildiz, "A new wireless communication paradigm through software-controlled metasurfaces," *IEEE Commun. Mag.*, vol. 56, no. 9, pp. 162–169, Sep. 2018.

[5] M. Di Renzo *et al.*, "Smart radio environments empowered by AI reconfigurable meta-surfaces: An idea whose time has come," Mar. 2019, *arXiv:1903.08925*. [Online]. Available: http://arxiv.org/abs/1903.08925

[6] E. Basar, M. Di Renzo, J. De Rosny, M. Debbah, M.-S. Alouini, and R. Zhang, "Wireless communications through reconfigurable intelligent surfaces," *IEEE Access*, vol. 7, pp. 116753–116773, Aug. 2019.

[7] S. Gong *et al.*, "Towards smart wireless communications via intelligent reflecting surfaces: A contemporary survey," *IEEE Commun. Surveys Tuts.*, early access, Jun. 22, 2020, doi: 10.1109/COMST.2020.3004197.

[8] Q. Wu and R. Zhang, "Towards smart and reconfigurable environment: Intelligent reflecting surface aided wireless network," *IEEE Commun. Mag.*, vol. 58, no. 1, pp. 106–112, Jan. 2020.

[9] J. Zhao, "Optimizations with intelligent reflecting surfaces (IRSs) in 6G wireless networks: Power control, quality of service, max-min fair beamforming for unicast, broadcast, and multicast with multi-antenna mobile users and multiple IRSs," Aug. 2019, *arXiv:1908.03965*. [Online]. Available: http://arxiv.org/abs/1908.03965

[10] Q. Wu and R. Zhang, "Intelligent reflecting surface enhanced wireless network via joint active and passive beamforming," *IEEE Trans. Wireless Commun.*, vol. 18, no. 11, pp. 5394–5409, Nov. 2019.

[11] X. Yu, D. Xu, and R. Schober, "MISO wireless communication systems via intelligent reflecting surfaces," in *Proc. IEEE/CIC Int. Conf. Commun. China (ICCC)*, Changchun, China, Aug. 2019, pp. 1–6.

[12] A. Zappone, M. Di Renzo, F. Shams, X. Qian, and M. Debbah, "Overhead-aware design of reconfigurable intelligent surfaces in smart radio environments," *IEEE Trans. Wireless Commun.*, early access, Sep. 2020, doi: 10.1109/TWC.2020.3023578.

[13] Q. Wu and R. Zhang, "Weighted sum power maximization for intelligent reflecting surface aided SWIPT," *IEEE Wireless Commun. Lett.*, vol. 9, no. 5, pp. 586–590, May 2020.

[14] Y. Han, W. Tang, S. Jin, C.-K. Wen, and X. Ma, "Large intelligent surface-assisted wireless communication exploiting statistical CSI," *IEEE Trans. Veh. Technol.*, vol. 68, no. 8, pp. 8238–8242, Aug. 2019.

[15] J. Ye, S. Guo, and M.-S. Alouini, "Joint reflecting and precoding designs for SER minimization in reconfigurable intelligent surfaces assisted MIMO systems," *IEEE Trans. Wireless Commun.*, vol. 19, no. 8, pp. 5561–5574, Aug. 2020.

[16] N. S. Perović, M. D. Renzo, and M. F. Flanagan, "Channel capacity optimization using reconfigurable intelligent surfaces in indoor mmWave environments," in *Proc. IEEE Int. Conf. Commun. (ICC)*, Dublin, Ireland, Jun. 2020, pp. 1–6.

[17] C. Huang, A. Zappone, M. Debbah, and C. Yuen, "Achievable rate maximization by passive intelligent mirrors," in *Proc. IEEE Int. Conf. Acoust., Speech Signal Process. (ICASSP)*, Calgary, AB, Canada, Apr. 2018, pp. 1–5.

[18] C. Pan *et al.*, "Multicell MIMO communications relying on intelligent reflecting surfaces," *IEEE Trans. Wireless Commun.*, vol. 19, no. 8, pp. 5218–5233, Aug. 2020.

[19] H. Li, R. Liu, M. Liy, Q. Liu, and X. Li, "IRS-enhanced wideband MU-MISO-OFDM communication systems," in *Proc. IEEE Wireless Commun. Netw. Conf. (WCNC)*, Seoul, South Korea, May 2020, pp. 1–6.

[20] C. Huang, A. Zappone, G. C. Alexandropoulos, M. Debbah, and C. Yuen, "Reconfigurable intelligent surfaces for energy efficiency in wireless communication," *IEEE Trans. Wireless Commun.*, vol. 18, no. 8, pp. 4157–4170, Aug. 2019.

[21] M. Cui, G. Zhang, and R. Zhang, "Secure wireless communication via intelligent reflecting surface," *IEEE Wireless Commun. Lett.*, vol. 8, no. 5, pp. 1410–1414, Oct. 2019.

[22] H. Shen, W. Xu, S. Gong, Z. He, and C. Zhao, "Secrecy rate maximization for intelligent reflecting surface assisted multi-antenna communications," *IEEE Commun. Lett.*, vol. 23, no. 9, pp. 1488–1492, Sep. 2019.

[23] X. Yu, D. Xu, and R. Schober, "Enabling secure wireless communications via intelligent reflecting surfaces," in *Proc. IEEE Global Commun. Conf. (GLOBECOM)*, Waikoloa, HI, USA, Dec. 2019, pp. 1–6.

[24] E. Björnson, O. Özdogan, and E. G. Larsson, "Intelligent reflecting surface versus decode-and-forward: How large surfaces are needed to beat relaying?" *IEEE Wireless Commun. Lett.*, vol. 9, no. 2, pp. 244–248, Feb. 2020.

[25] H. Zhang, B. Di, L. Song, and Z. Han, "Reconfigurable intelligent surfaces assisted communications with limited phase shifts: How many phase shifts are enough?" *IEEE Trans. Veh. Technol.*, vol. 69, no. 4, pp. 4498–4502, Apr. 2020.

[26] Q. Wu and R. Zhang, "Beamforming optimization for wireless network aided by intelligent reflecting surface with discrete phase shifts," *IEEE Trans. Commun.*, vol. 68, no. 3, pp. 1838–1851, Mar. 2020.

[27] S. Abeywickrama, R. Zhang, Q. Wu, and C. Yuen, "Intelligent reflecting surface: Practical phase shift model and beamforming optimization," *IEEE Trans. Commun.*, vol. 68, no. 9, pp. 5849–5863, Sep. 2020.

[28] W. Cai, H. Li, M. Li, and Q. Liu, "Practical modeling and beamforming for intelligent reflecting surface aided wideband systems," *IEEE Commun. Lett.*, vol. 24, no. 7, pp. 1568–1571, Jul. 2020.

[29] B. Di, H. Zhang, L. Li, L. Song, Y. Li, and Z. Han, "Practical hybrid beamforming with finite-resolution phase shifters for reconfigurable intelligent surface based multi-user communications," *IEEE Trans. Veh. Technol.*, vol. 69, no. 4, pp. 4565–4570, Apr. 2020.

[30] M.-A. Badiu and J. P. Coon, "Communication through a large reflecting surface with phase errors," *IEEE Wireless Commun. Lett.*, vol. 9, no. 2, pp. 184–188, Feb. 2020.

[31] E. Basar, "Reconfigurable intelligent surface-based index modulation: A new beyond MIMO paradigm for 6G," *IEEE Trans. Commun.*, vol. 68, no. 5, pp. 3187–3196, May 2020.

[32] W. Yan, X. Yuan, Z.-Q. He, and X. Kuai, "Passive beamforming and information transfer design for reconfigurable intelligent surfaces aided multiuser MIMO systems," *IEEE J. Sel. Areas Commun.*, vol. 38, no. 8, pp. 1793–1808, Aug. 2020.

[33] R. Liu, H. Li, M. Li, and Q. Liu, "Symbol-level precoding design for intelligent reflecting surface assisted multi-user MIMO systems," in *Proc. 11th Int. Conf. Wireless Commun. Signal Process. (WCSP)*, Xian, China, Oct. 2019, pp. 1–6.

[34] C. Huang *et al.*, "Holographic MIMO surfaces for 6G wireless networks: Opportunities, challenges, and trends," *IEEE Wireless Commun.*, early access, Jul. 8, 2020, doi: 10.1109/MWC.001.1900534.

[35] K. Yang, Y. Shi, Y. Zhou, Z. Yang, L. Fu, and W. Chen, "Federated machine learning for intelligent IoT via reconfigurable intelligent surface," *IEEE Netw.*, vol. 34, no. 5, pp. 16–22, Sep. 2020.

[36] C. Huang, R. Mo, and C. Yuen, "Reconfigurable intelligent surface assisted multiuser MISO systems exploiting deep reinforcement learning," *IEEE J. Sel. Areas Commun.*, vol. 38, no. 8, pp. 1839–1850, Aug. 2020.

[37] J. Chen, Y.-C. Liang, H. V. Cheng, and W. Yu, "Channel estimation for reconfigurable intelligent surface aided multi-user MIMO systems," Dec. 2019, *arXiv:1912.03619*. [Online]. Available: http://arxiv.org/abs/1912.03619

[38] C. Hu and L. Dai, "Two-timescale channel estimation for reconfigurable intelligent surface aided wireless communications," Dec. 2019, *arXiv:1912.07990*. [Online]. Available: http://arxiv.org/abs/1912.07990

[39] C. You, B. Zheng, and R. Zhang, "Channel estimation and passive beamforming for intelligent reflecting surface: Discrete phase shift and progressive refinement," *IEEE J. Sel. Areas Commun.*, early access, Jul. 3, 2020, doi: 10.1109/JSAC.2020.3007056.

[40] L. Wei, C. Huang, G. C. Alexandropoulos, and C. Yuen, "Parallel factor decomposition channel estimation in RIS-assisted multi-user MISO communication," in *Proc. IEEE 11th Sensor Array Multichannel Signal Process. Workshop (SAM)*, Hangzhou, China, Jun. 2020, pp. 1–5.

[41] M. Alodeh, S. Chatzinotas, and B. Ottersten, "Constructive multiuser interference in symbol level precoding for the MISO downlink channel," *IEEE Trans. Signal Process.*, vol. 63, no. 9, pp. 2239–2252, May 2015.

[42] C. Masouros and G. Zheng, "Exploiting known interference as green signal power for downlink beamforming optimization," *IEEE Trans. Signal Process.*, vol. 63, no. 14, pp. 3628–3640, Jul. 2015.

[43] M. Alodeh *et al.*, "Symbol-level and multicast precoding for multiuser multiantenna downlink: A state-of-the-art, classification, and challenges," *IEEE Commun. Surveys Tuts.*, vol. 20, no. 3, pp. 1733–1757, 3rd Quart., 2018.

[44] A. Li and C. Masouros, "Interference exploitation precoding made practical: Optimal closed-form solutions for PSK modulations," *IEEE Trans. Wireless Commun.*, vol. 17, no. 11, pp. 7661–7676, Nov. 2018.

[45] A. Li *et al.*, "A tutorial on interference exploitation via symbol-level precoding: Overview, State-of-the-Art and future directions," *IEEE Commun. Surveys Tuts.*, vol. 22, no. 2, pp. 796–839, 2nd Quart., 2020.

[46] A. Ben-Tal and A. Nemirovski, *Lectures on Modern Convex Optimization: Analysis, Algorithms, and Engineering Applications*, Philadelphia, PA, USA: Society for Industrial and Applied Mathematics, 2001.

[47] N. Boumal, B. Mishra, P.-A. Absil, and R. Sepulchre, "Manopt, a MATLAB toolbox for optimization on manifolds," *J. Mach. Learn. Res.*, vol. 15, pp. 1455–1459, Aug. 2014.
[48] J. R. Shewchuk. (1994). *An Introduction to the Conjugate Gradient Method Without the Agonizing Pain*. [Online]. Available: http://www.cs.cmu.edu/%7Equake-papers/painless-conjugate-gradient.pdf
[49] A. Wiesel, Y. C. Eldar, and S. Shamai, "Linear precoding via conic optimization for fixed MIMO receivers," *IEEE Trans. Signal Process.*, vol. 54, no. 1, pp. 161–176, Jan. 2006.

Rang Liu (Graduate Student Member, IEEE) received the B.S. degree in electronics information engineering from the Dalian University of Technology, Dalian, China, in 2018, where she is currently pursuing the Ph.D. degree with the School of Information and Communication Engineering.

Her current research interests include on signal processing, mmWave communications, and massive MIMO systems.

Ming Li (Senior Member, IEEE) received the M.S. and Ph.D. degrees in electrical engineering from the State University of New York at Buffalo (SUNY-Buffalo), Buffalo, in 2005 and 2010, respectively.

From January 2011 to August 2013, he was a Post-Doctoral Research Associate with the Signals, Communications, and Networking Research Group, Department of Electrical Engineering, SUNY-Buffalo. From August 2013 to June 2014, he joined Qualcomm Technologies Inc., as a Senior Engineer. Since June 2014, he has been with the School of Information and Communication Engineering, Dalian University of Technology, Dalian, China, where he is currently an Associate Professor. His current research interests include the general areas of communication theory and signal processing with applications to mmWave communications, secure wireless communications, cognitive radios and networks, data hiding, and steganography.

Qian Liu (Member, IEEE) received the B.S. and M.S. degrees from the Dalian University of Technology, Dalian, China, in 2006 and 2009, respectively, and the Ph.D. degree from The State University of New York at Buffalo (SUNY-Buffalo), Buffalo, NY, USA, in 2013.

She was a Post-Doctoral Fellow with the Ubiquitous Multimedia Laboratory, SUNY-Buffalo, from 2013 to 2015. She was a Post-Doctoral Fellow with the Chair of Media Technology and the Chair of Communication Networks, Technical University of Munich, from 2016 to 2017. She is currently an Associate Professor with the School of Computer Science and Technology, Dalian University of Technology. Her current research interests include multimedia transmission over MIMO systems, IEEE 802.11 wireless networks and LTE networks, device-to-device communication, energy-aware multimedia delivery, and the Tactile Internet. She received the Alexander von Humboldt Fellowship in 2015. She received the Best Paper Runner-Up Award at the 2012 IEEE International Conference on Multimedia and Expo and was in the finalist for the Best Student Paper Award at the 2011 IEEE International Symposium on Circuits and Systems.

A. Lee Swindlehurst (Fellow, IEEE) received the B.S. and M.S. degrees in electrical engineering from Brigham Young University (BYU), in 1985 and 1986, respectively, and the Ph.D. degree in electrical engineering from Stanford University in 1991. He was with the Department of Electrical and Computer Engineering, BYU, from 1990 to 2007, where he served as the Department Chair from 2003 to 2006. From 1996 to 1997, he held a joint appointment as a Visiting Scholar with Uppsala University and the Royal Institute of Technology, Sweden. From 2006 to 2007, he was on leave working as the Vice President of Research for ArrayComm LLC, San Jose, CA, USA. Since 2007, he has been a Professor with the Electrical Engineering and Computer Science Department, University of California at Irvine, where he served as an Associate Dean for Research and Graduate Studies with the Samueli School of Engineering from 2013 to 2016. From 2014 to 2017, he was also a Hans Fischer Senior Fellow with the Institute for Advanced Studies, Technical University of Munich. In 2016, he was elected as a Foreign Member of the Royal Swedish Academy of Engineering Sciences (IVA). His research interests include array signal processing for radar, wireless communications, and biomedical applications, and he has over 300 publications in these areas. He was the inaugural Editor-in-Chief of the IEEE JOURNAL OF SELECTED TOPICS IN SIGNAL PROCESSING. He received the 2000 IEEE W. R. G. Baker Prize Paper Award, the 2006 IEEE Communications Society Stephen O. Rice Prize in the Field of Communication Theory, the 2006 and 2010 IEEE Signal Processing Society's Best Paper Awards, and the 2017 IEEE Signal Processing Society Donald G. Fink Overview Paper Award.